# Design and experimental verification of a dual-band metamaterial filter*

Hong-Yang Zhu(朱洪杨)[1], Ai-Qin Yao(姚爱琴)[1], and Min Zhong(钟敏)[2,†]

[1] North University of China, Taiyuan 030051, China
[2] Hezhou University, Hezhou 542899, China

(Received 11 March 2016; revised manuscript received 16 June 2016; published online 25 August 2016)

In this paper, we present the design, simulation, and experimental verification of a dual-band free-standing metamaterial filter operating in a frequency range of 1 THz–30 THz. The proposed structure consists of periodically arranged composite air holes, and exhibits two broad and flat transmission bands. To clarify the effects of the structural parameters on both resonant transmission bands, three sets of experiments are performed. The first resonant transmission band shows a shift towards higher frequency when the side width $w_1$ of the main air hole is increased. In contrast, the second resonant transmission band displays a shift towards lower frequency when the side width $w_2$ of the sub-holes is increased, while the first resonant transmission band is unchanged. The measured results indicate that these resonant bands can be modulated individually by simply optimizing the relevant structural parameters ($w_1$ or $w_2$) for the required band. In addition, these resonant bands merge into a single resonant band with a bandwidth of 7.7 THz when $w_1$ and $w_2$ are optimized simultaneously. The structure proposed in this paper adopts different resonant mechanisms for transmission at different frequencies and thus offers a method to achieve a dual-band and low-loss filter.

**Keywords:** photoelectric, metamaterial, filter

**PACS:** 73.20.Mf, 41.20.Jb, 78.20.Mg **DOI:** 10.1088/1674-1056/25/10/107301

## 1. Introduction

In recent years, artificially prepared metamaterial devices have demonstrated unique electromagnetic properties that originate from the coupled interaction between electromagnetic waves and designed periodic arrays of sub-wavelength air holes.[1–5] Of these designed metamaterial structures, self-symmetric metal/dielectric/metal composite multilayer nanostructures have been studied most widely, both numerically and experimentally.[6–10] This is because this configuration offers enormous modulation flexibility over the effective medium parameters (including the effective permeability, effective permittivity and effective impedance). In particular, composite multilayer fishnet nanostructures are experimentally demonstrated at optical and infrared wavelengths through patterning nano-scale air holes in composite multilayer stacks, which are subsequently deposited on different types of substrates by reactive ion etching (RIE), focused ion beam (FIB) etching, or metal lift-off techniques.[11–13] Many experiments have been carried out based on substrate-mounted hollow fishnet composite multilayer nanostructures with non-ideal tapered sidewalls. Measured results proved the existence of the asymmetric reflections, which must be measured from the opposing interfaces of the designed device because of the occurrence of nonzero magneto-electric coupling.[14] Unfortunately, the supporting substrate and the sidewall angle induced in the fabrication process[15–19] may result in the undesirable broken symmetry in the metamaterial device. This broken symmetry damages the effective medium model because the electric and magnetic polarizations of the model are characterized based on the electric and magnetic field components. It is therefore necessary to develop a metamaterial device that does not require substrate supporting. Moreover, the unique optical properties of the designed metamaterial device are dependent on the specific structural design, which is aligned using the periodic lattice.[20] The optical properties of the designed structure are related to the effective permeability and permittivity, which in turn are strongly dependent on the resonant frequency. This optically dispersive behavior always results in the distortion of the electromagnetic signal and narrow operable bandwidth,[21–24] which naturally restricts the widespread applications of the designed metamaterial device in practice. Therefore, a new nanostructure with non-substrate supporting should be developed to tailor the dispersive behavior of the structure and obtain both low loss and broad bandwidth characteristics, which still satisfy the strict constraints of the nanofabrication approach.

In this paper, we present the numerical and experimental verification of an optically functional metamaterial filter in a three-layer metal–dielectric free-standing configuration that is optimized to produce dual-band properties in a 1 THz–30 THz

*Project supported by the Doctorate Scientific Research Foundation of Hezhou University, China (Grant No. HZUBS201503), the Promotion of the Basic Ability of Young and Middle-aged Teachers in Universities Project of Guangxi Zhuang Autonomous Region, China (Grant No. KY2016YB453), the Guangxi Colleges and Universities Key Laboratory Symbolic Computation, China, Engineering Data Processing and Mathematical Support Autonomous Discipline Project of Hezhou University, China (Grant No. 2016HZXYSX01).

†Corresponding author. E-mail: zhongmin2012hy@163.com

© 2016 Chinese Physical Society and IOP Publishing Ltd 

wave spectral window, and highly reflective behavior outside these bands. This non-hollow fishnet structure shapes the resonant dispersion behaviors of the effective permeability and effective permittivity to satisfy the dual- and flat-band transmission demands. These effective parameters are extracted from the measured transmission and reveal magnetic–electric coupling in these plasmonic resonant bands. The measured transmission of the proposed free-standing structure agrees well with the simulated result, which confirms that this non-hollow fishnet structure can be produced for dual-band metamaterial filter applications. In addition, these resonant bands can be modulated individually. This useful structural design overcomes the limitations of narrow bandwidths, which can thus distinctly increase the available possibilities for practical optical device manufacture.

## 2. Structural design, simulation method, and experimental details

The proposed structure is composed of a metal/dielectric stack with a compound square air hole array that perforates all silver layers as shown in Fig. 1. The thickness values of the silver, SU-8, and polyimide layers are $h_1 = 0.04$ μm, $h_2 = 0.18$ μm, and $h_3 = 0.18$ μm, respectively, which leads to a total metamaterial thickness of 0.44 μm. The periodicity of the proposed structure is $P = 12$ μm, and the widths of the main air hole and the sub-holes are $w_1 = 4.5$ μm and $w_2 = 1$ μm, respectively. The optical properties of the proposed structure are calculated by using a full-wave electromagnetic solver (Ansoft 13.0). In the simulations, Floquet ports are used at the bottom and top boundaries of the unit cell to simulate a normally-incident electromagnetic wave, and the periodic boundary conditions are used for the four sidewalls.

To validate the proposed design, the dual-band metamaterial filter is fabricated by the following procedure: a 0.04-μm-thick bottom silver layer is evaporated on a thermally oxidized Si handle substrate at a rate of 1.8 Å·s$^{-1}$ by electron beam evaporation (ZZL-U400H). A 0.18-μm-thick polyimide layer is deposited on the bottom silver layer by spin-coating a polyimide precursor at a speed of 1950 rpm for 28 s (HD Microsystem PI2556). The polyimide layer is imidized by heating at 135 °C for 38 min and then at 220 °C for 70 min by using a nitrogen-purged convection oven. A 0.18-μm-thick SU-8 layer is then spun on the polyimide layer (MSC-400Bz-6N). The SU-8 layer is baked at 100 °C for 75 s (C-MAG HP10). Another 0.04-μm-thick top silver layer is evaporated on the intermediate dielectric layer. The fabricated metal/dielectric structure is subsequently removed from the substrate by using a buffered oxide etchant to etch the underlying thermal oxide away. The designed main and nano-notch air hole array is patterned on the top and bottom silver layers using a focused ion beam system[25] (Helios nanolab 600). The measured transmission of the designed structure is achieved (Bruker Optics Equinox 55 Fourier transform infrared spectrometer), and the optical microscopy image of the free-standing dual-band metamaterial filter is obtained (Leica DM4M) as shown in Fig. 1(c). The measured results indicate that two resonant transmission bands are obtained, which are simply named the "first" and "second" bands, as shown in Fig. 1(c).

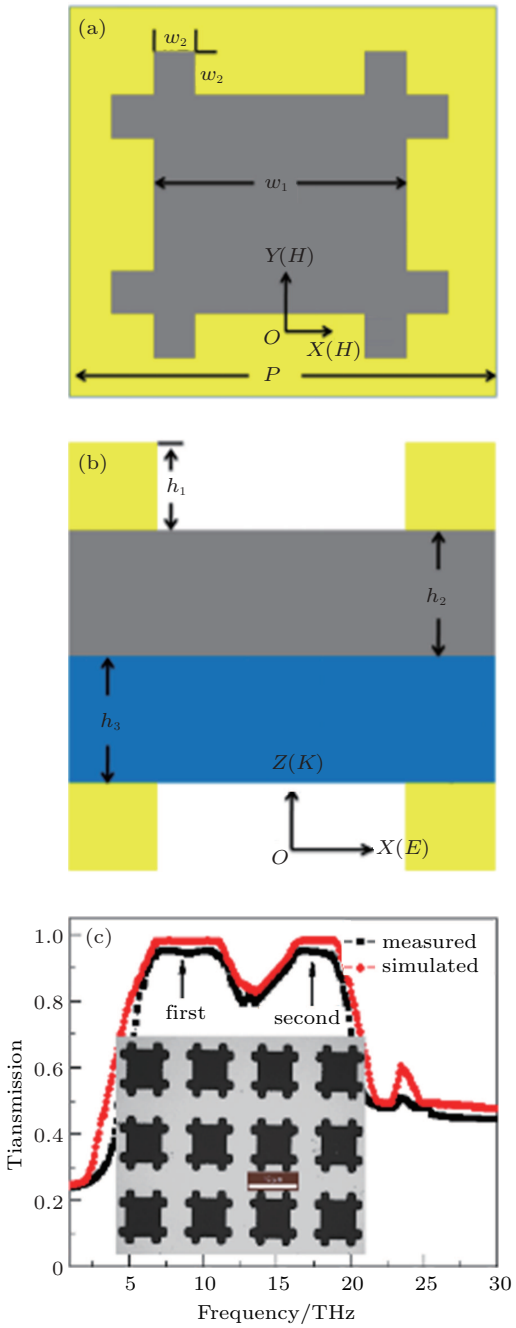



**Fig. 1.** (color online) (a) Top view on the *xoy* plane. (b) Side view on the *xoz* plane. The yellow part is the silver layer, the gray part is the polyimide layer, the blue part is the SU-8 layer. (c) The measured and simulated transmission spectra, and the inset shows a photograph of the samples.

## 3. Optical properties of the dual-band metamaterial filter

The optical properties of the proposed structure can be understood through examining the effective medium parameters as shown in Fig. 2. These parameters can offer an in-

sight into how the magnetic and electric responses of the proposed structure vary with frequency, which are nonlocal in nature.[26] The proposed structure dispersion behavior can be tailored through adjusting the permeability profile in the Drude mode[27] with a plasma frequency $f_e$. The effective permeability $\mu_{\rm eff}(f)$ and permittivity $\varepsilon_{\rm eff}(f)$ could be expressed in the following form:

$$\varepsilon(\omega) = 1 - \frac{\omega_p^2}{\omega^2 - i\omega\gamma_D}, \tag{1}$$

$$\mu_{\rm eff}(f) = \mu_0 \left(1 - \sum_{i=1}^{2} \frac{F_i c_0^2/f_e^2}{c_0^2/f^2 - c_0^2/f_{mi}^2 - jc_0\gamma_{mi}/f_{mi}}\right), \tag{2}$$

$$\varepsilon_{\rm eff}(f) = \varepsilon_0 \left(\varepsilon_\infty - \frac{c_0^2/f_e^2}{c_0^2/f^2 - jc_0\gamma_e/f}\right). \tag{3}$$

The effective impedance could be given by

$$Z_{\rm eff}(f) = \sqrt{\mu_{\rm eff}(f)/\varepsilon_{\rm eff}(f)}. \tag{4}$$

Here, $\omega_p = 1.37 \times 10^{16}$ s$^{-1}$ is the plasma frequency, $\gamma_D = 9 \times 10^{13}$ s$^{-1}$ is the collision frequency,[28] $\gamma_i$ is the damping factor, $F_i$ is the filling factor, $c_0 = 3.0 \times 10^8$ m/s is the speed of light in free space, $\varepsilon_0 = 8.85 \times 10^{-12}$ C/(N·m$^2$) is the permittivity of vacuum, and $f_{mi}$ is the frequency associated with the resonance.[29] In our simulations, two ideal magnetic conductor planes are adopted on the boundaries which are normal to the $x$ axis, then two ideal electric conductor planes are used on the boundaries which are normal to the y axis.[30] As shown in Fig. 2(a), the real part of the effective permeability shows a strong magnetic resonance around 9 THz in the first transmission band, and a magnetic resonance around 18 THz in the second transmission band. In the first band, the relative strength of the magnetic resonance leads to a resonance of the effective permittivity. Similarly, in the second band, the effective permittivity of the proposed structure shows an anti-resonance.[26] The real part of the effective impedance is given by

$$Z_{\rm eff}(f) = \sqrt{\mu_{\rm eff}(f)/\varepsilon_{\rm eff}(f)} = Z_0, \tag{5}$$

where the $Z_{\rm eff}(f)$ is matched to the value for free space in the first and second bands. Two broad and flat pass-bands with near-ideal transmission are obtained as shown in Fig. 1. Outside these transmission bands, the real parts of the permeability and permittivity are imbalanced, which results in blocking the wave transmission. The imaginary parts of the permeability and permittivity are shown in Fig. 2(b). On the one hand, the imaginary parts of the permeability and permittivity are minimized in these transmission bands, which causes the designed metamaterial filter to have a low absorption loss as shown in Fig. 2(b). On the other hand, the real parts of the effective impedance are well-matched to that in free space in these transmission bands, which leads to low reflection loss across the bands. However, outside these transmission bands, the effective impedance is mismatched, and this is responsible for the strong reflection losses outside these bands.

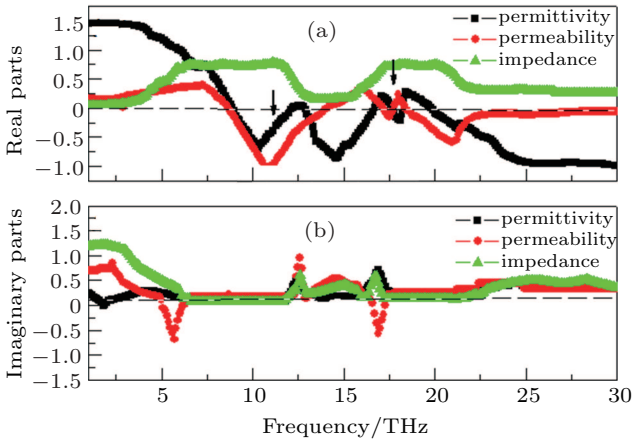



**Fig. 2.** (color online) Simulated (a) real and (b) imaginary parts of effective medium parameters (permittivity, permeability, and impedance) versus frequency.

To investigate the electromagnetic responses of these transmission bands, the current distributions on the top and bottom layers of the designed structure are calculated, and the results are shown in Fig. 3. The resonant electromagnetic response, which results in the dual-band filtering properties, can be understood through an analysis of the calculated volumetric current distributions. For the fundamental magnetic resonance mode of the first band, parallel current flows can be observed on the top and bottom silver layer as shown in Figs. 3(a) and 3(b).

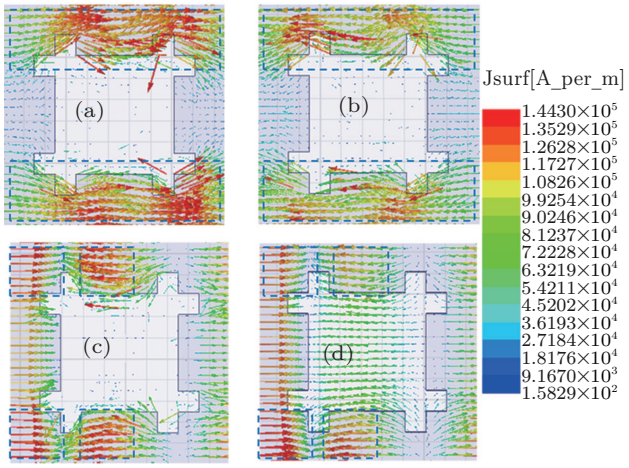



**Fig. 3.** (color online) Volumetric current density distributions of the proposed structure at the two magnetic resonance modes. (a) The top silver layer at 9 THz. (b) The bottom silver layer at 9 THz. (c) The top silver layer at 18 THz. (d) The bottom silver layer at 18 THz.

Clearly, the proposed structure shows nearly equal calculated current distributions on the bottom and top silver layers in the first band, and this indicates that neither magnetic nor electric dipole moments are excited by the electric/magnetic fields. The calculated current distributions for the first magnetic resonant mode generate charge accumulation, directional flow, and depletion in an elongated region (dotted line areas) along the edges of the main air hole area of the unit cell as shown in Figs. 3(a) and 3(b). For the second band, anti-parallel current flows can be observed as shown in Figs. 3(c) and 3(d).

These anti-parallel current flows are mainly distributed in the square-like regions (dotted line areas) along the $x$ direction between the sub-holes, with a phase difference of 180°. This produces square-like charge accumulation, directional flow, and depletion regions between the sub-holes with different current phases, which indicate that the magnetic resonant mode of the second band can mainly be attributed to these anti-parallel currents.[31]

To assess the effects of the structural parameters on the transmission bands, three set of experiments are carried out: the first set is for varying air hole width ($w_1$) with sub-hole width ($w_2$) fixed, the second set is for varying $w_2$ with $w_1$ fixed, and the third set is for varying $w_1$ and $w_2$ simultaneously.

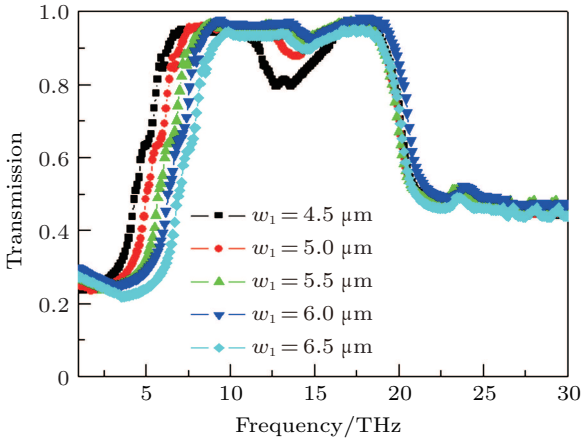



**Fig. 4.** (color online) Measured transmission spectra of the designed structure for different values of $w_1$ ($w_2 = 1$ μm).

In the proposed structure, the structural parameters $w_1$ and $w_2$ can naturally affect the optical properties. To obtain an optimized dual-band structural design, the effects of these factors are experimentally investigated. In the first set of experiments as shown in Fig. 4, $w_1$ is increased from 4.5 μm to 6.5 μm while $w_2$ remains constant. The first transmission band displays a shift towards higher frequency. It is obvious that an increase in $w_1$ results in the bandwidth initially 4.0 THz ($w_1 =$ 4.5 μm) increasing, reaching a maximum bandwidth 6.3 THz ($w_1 = 6.0$ μm), and then decreasing to 3.9 THz ($w_1 = 6.5$ μm) as shown in Fig. 4. Additionally, the corresponding simulation results are shown in Fig. 5, which also confirms the effect of the $w_1$ on the first transmission band. However, the bandwidth and the resonant frequency of the second band remain almost unchanged with $w_1$ increasing. Based on previous discussion, this shows that an effective impedance matching condition is achieved in the first band. When $w_1$ is increased from $w_1 = 4.5$ μm to $w_1 = 5.5$ μm, the impedance matching condition between the designed structure and the free air is improved. When $w_1 = 6.0$ μm, the perfect impedance matching condition is obtained[32] in the first transmission band, which leads to the maximum bandwidth as indicated in Figs. 4 and 5. Therefore, the perfect impedance matching condition will be damaged for $w_1 > 6.0$ μm, which results in the reduction of the bandwidth of the first band shown in Figs. 4 and 5. These measured and simulated results in Figs. 4 and 5 indicate that there is an optimum $w_1 = 6.0$ μm to obtain the maximum bandwidth of the first transmission band. These measured results indicate that the effective impedance matching condition is possibly determined by the side width $w_1$ of the main air hole in the first band. Therefore, an increase in $w_1$ would result in a higher impedance matching between the air interface and the top silver layer, which then leads to the reflection reducing and the bandwidth expanding[32] as shown in Fig. 4.

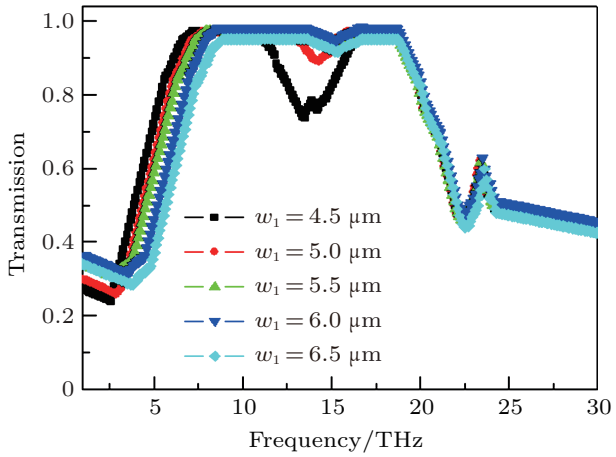



**Fig. 5.** (color online) Simulated transmission spectra of the designed structure for different values of $w_1$ ($w_2 = 1$ μm).

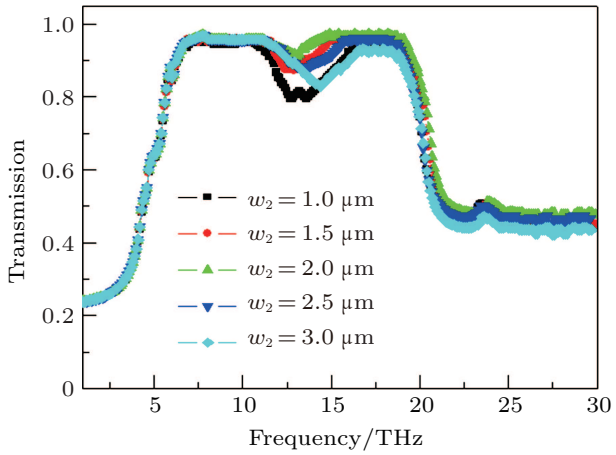



**Fig. 6.** (color online) Measured transmission spectra of the designed structure with $w_1 = 4.5$ μm for different values of $w_2$.

The second set of experiments is carried out in a similar manner as shown in Fig. 6. The side width $w_2$ of the sub-hole is increased from $w_2 = 1.0$ μm to $w_2 = 3.0$ μm while $w_1$ remains constant. The second band displays an obvious shift towards lower frequency. It is obvious that the bandwidth of the second band is increased from 3.0 THz ($w_2 = 1.0$ μm) to 4.8 THz ($w_2 = 2.0$ μm), then reduced to 2.7 THz ($w_2 =$ 3.0 μm). It is because the impedance matching condition is improved in the second transmission band with $w_2$ increasing. When $w_2$ is increased from $w_2 = 1.0$ μm to $w_2 = 2.0$ μm, the perfect impedance matching condition is obtained[32] in the second transmission band, which results in the maximum

bandwidth in Figs. 6 and 7. This is similar to the results in Figs. 4 and 5. This occurs because the effective impedance matching condition in the second band is mainly determined by the side width $w_2$. These resonant bands could therefore be modulated individually by optimizing the individual structural parameters $(w_1, w_2)$.

The third set of experiments is carried out by simultaneously increasing both structural parameters $(w_1, w_2)$ to demonstrate the effects of these parameters on the resonant bands of the designed filter.

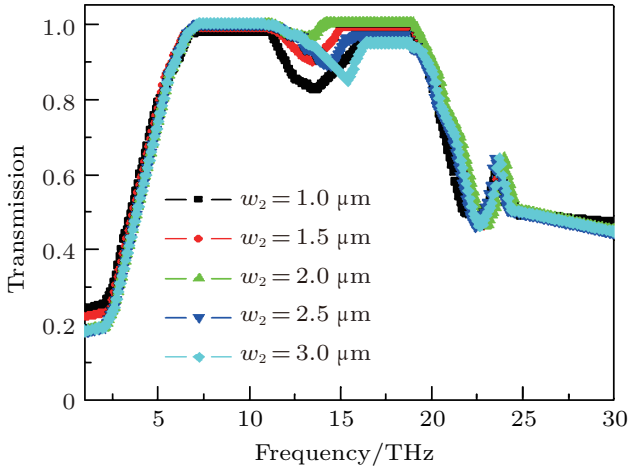



**Fig. 7.** (color online) Simulated transmission spectra of the designed structure with $w_1 = 4.5$ μm for different values of $w_2$.

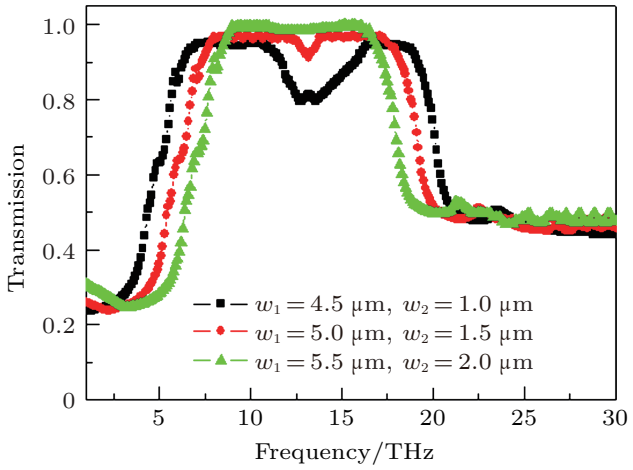



**Fig. 8.** (color online) Measured transmission spectra of the designed structure with different values of $w_1$ and $w_2$.

Figure 8 shows the transmission spectra measured when $w_1$ and $w_2$ are optimized simultaneously. The bandwidths of both bands are increased, and these resonant bands move closer to each other. When $w_1 = 5.5$ μm and $w_2 = 2$ μm, the first and the second bands merge into a single resonant band with a bandwidth of 7.7 THz as shown in Fig. 8. The simulated results in Fig. 9 are similar to those in Fig. 8. It is because the effective perfect impedance matching conditions in the first and the second bands are achieved simultaneously when $w_1 = 5.5$ μm and $w_2 = 2$ μm. These measured and simulated results indicate that the impedance matching condition of the proposed structure is mainly determined by these structural parameters.

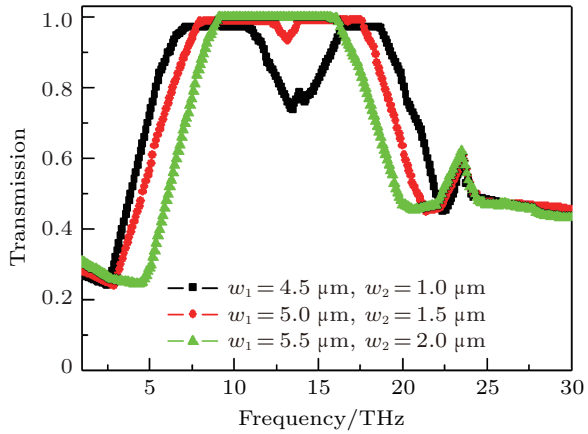



**Fig. 9.** (color online) Simulated transmission spectra of the designed structure with different values of $w_1$ and $w_2$.

## 4. Conclusions

In this work, we experimentally study a dual-band metamaterial filter. The first resonant band is expanded and shifts to higher frequency by increasing $w_1$ alone. The second resonant band is expanded and shifts to lower frequency by increasing $w_2$ alone. Further experimental studies indicate that the first and second band can be modulated to move closer to each other together and merge into a single transmission band by simultaneously optimizing the two structural parameters. This experimental demonstration verifies that the proposed free-standing non-hollow fishnet structure can be used to produce a new metamaterial filter with dual-band properties.

## References

[1] Xu H X, Wang G M, Wang J F and Yang Z M 2012 *Chin. Phys. B* **21** 124101
[2] Wan M L, Yuan S Q, Dai K J, Song Y L, Zhou F Q and He J N 2014 *Chin. Phys. B* **23** 107808
[3] Dimitriadis A, Kantartzis N and Tsiboukis T 2012 *Appl. Phys. A* **109** 1065
[4] Liu Y H, Gu S, Luo C R and Zhao X P 2009 *Appl. Phys. Lett.* **95** 241111
[5] Wen Q Y, Zhang H W, Yang Q H, Chen Z, Long Y, Jing Y L, Lin Y and Zhang P X 2012 *J. Phys. D: Appl. Phys.* **45** 235106
[6] Liu N, Guo H C, Fu L W, Kaiser S, Schweizer H and Giessen H 2008 *Nat. Mater.* **7** 31
[7] Tuong P V, Lam V D, Park J W, Choi E H, NikitovS A and Lee Y P 2013 *Photonics and Nanostructures–Fundamentals and Applications* **11** 89
[8] Wei Z Y, Cao Y, Han J, Wu C, Fan Y C and Li H Q 2010 *Appl. Phys. Lett.* **97** 141901
[9] Cheng Y Z, Nie Y and Gong R Z 2013 *Opt. Laser Technol.* **48** 415
[10] Wang C N, Bai M, Jin M and Zhang Y F 2012 *Optik* **123** 1820
[11] Chanda D, Shigeta K, Gupta S, Cain T, Carlson A, Mihi A, Baca A J, Bogart G R, Braun P and Rogers J A 2011 *Nat. Nanotechnol.* **6** 402
[12] Valentine J, Zhang S, Zentgraf T, Ulin-Avila E, Genov D A, Bartal G and Zhang X 2008 *Nature* **455** 376
[13] Zhang S, Fan W, Panoiu N C, Malloy K J, Osgood R M and Brueck S R J, 2005 *Phys. Rev. Lett.* **95** 137404
[14] Ku Z and Brueck S R J 2009 *Appl. Phys. Lett.* **94** 153107
[15] Albooyeh M and Simovski C R 2011 *J. Opt.* **13** 105102
[16] Jiang Z H and Werner D H 2013 *Opt. Express* **21** 5594
[17] Powell D A and Kivshar Y S 2010 *Appl. Phys. Lett.* **97** 091106

[18] Ku Z, Zhang J and Brueck S R J 2009 *Opt. Express* **17** 6782
[19] Kildishev A V, Borneman J D, Ni X, Shalaev V M and Drachev V P 2011 *Proc. IEEE* **99** 1691
[20] Kschny T, Kafesaki M, Economou E N and Soukoulis C M 2004 *Phys. Rev. Lett.* **93** 107402
[21] Schurig D, Mock J J, Justice B J, Cummer S A, Pendry J B, Starr A F and Smith D R 2006 *Science* **314** 977
[22] Fang N, Lee H, Sun C and Zhang X 2005 *Science* **308** 534
[23] Grbic A and Eleftheriades G V 2004 *Phys. Rev. Lett.* **92** 117403
[24] Cai W S, Chettiar U K, Kildishev A V and Shalaev V M 2007 *Nat. Photon.* **1** 224
[25] Cheng F, Yang X D and Gao J 2014 *Opt. Lett.* **39** 3185
[26] Simovski C R and Tretyakov S A 2007 *Phys. Rev. B* **75** 195111
[27] Zhong M and Ye Y H 2015 *Opt. Commun.* **335** 94
[28] Zhang S, Fan W J, Paniou N C, Malley K J, Osgood R M and Brueck S R J 2005 *Phys. Rev. Lett.* **95** 137404
[29] Oughstun K E and Shen S 1988 *J. Opt. Soc. Am. B* **5** 2395
[30] Smith D R, Schult S, Markos P and Soukoulis C M 2002 *Phys. Rev. B* **65** 195104
[31] Yang J, Sauvan C, Liu H T and Lalanne P 2008 *Phys. Rev. Lett.* **107** 043903
[32] Landy N I, Sajuyigbe S, Mock J J, Smith D R and Padilla W J 2008 *Phys. Rev. Lett.* **100** 207402